A.F. Zarnecki
August 5/6, 2022

LUXE

3 August 2022

Electromagnetic calorimeter

LUXE collaboration

Summary

The electromagnetic calorimeters of the LUXE experiment are designed as sampling calorimeters using silicon sensors and tungsten absorber plates. They will measure the number of positrons and their energy spectrum in e-laser and γ-laser interactions or electrons in γ-laser interactions. In addition, they will be used for the cross-calibration of the energy scale with the tracker. In the following the mechanical structure, the sensors, the Front-End electronics and the DAQ are described. Monte Carlo simulations based on the GEANT4 package are used to estimate the performance of ECAL-P in terms of energy and position resolution, as well as for the reconstruction of the number of positrons impacting the ECAL-P and their energy spectrum. Similar studies for ECAL-E are planned.

LUXE Doc: xxx-yyy-zzzz
Version: 0.1
Last modified: 15:07 on 3 August 2022

Note Authors:

H. Abramowicz
W. Lohmann

Editorial Board:

G. Sarri
M. Bruschi
R. Pöschl

Contents

1 Introduction

The LUXE experiment will explore the uncharted territory of strong field quantum electrodynamics (SFQED) in e-laser and γ-laser interactions at an effective field strength at and above the Schwinger limit. In this regime, non-linear and non-pertubative effects are expected to appear in the production rates of electron-positron pairs. Hence, the number of electron-positron pairs and their energy distribution in e-laser and γ-laser interactions are key characteristics to probe SFQED. In the LUXE experiment, the schematic layouts of which is shown in Fig. 1, positrons originating from trident production in e-laser and from the Breit-Wheeler process γ-laser interactions will be measured in a detector system consisting of a tracker followed by an electromagnetic calorimeter, ECAL-P. The ECAL-P design is based on a technology for highly compact electromagnetic calorimeters which was developed by the FCAL collaboration [1, 2], an R&D collaboration to design, build and test prototypes of luminometers for future linear electron-positron colliders (ILC or CLIC). In the γ-laser setup, also the spectra of electrons originating from the Breit-

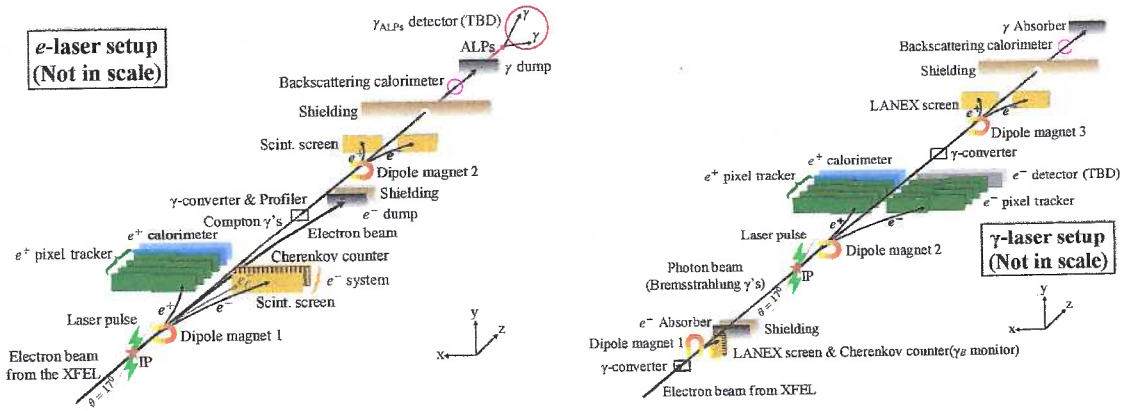

Figure 1: Schematic layouts for the e-laser and γ-laser setup. Shown are the magnets, detectors and main shielding and absorbing elements.

Wheeler process will be measured. For that purpose, the same tracker as for positrons will be followed by ECAL-E, a silicon-tungsten electromagnetic calorimeter based on the technology developed by the CALICE collaboration [3]. The highly granular ECAL-E is the reference design of the electromagnetic calorimeter for the International Large Detector (ILD) concept.

The tracker and both ECALs are located downstream of a dipole magnet which directs the positrons and electrons from the interaction point to the detectors. The correlation between the position and the energy of the positrons and electrons, determined by the dipole magnetic field, constitutes the basis for energy measurements in the tracker. By directly measuring the energy, the ECALs can determine whether more than one particle had almost the same path. Thus, the role of the ECALs is to determine, independently of the tracker, the number and energy spectra of eletrons and positrons. The combination will provide an independent in situ energy calibration. In addition, it will ensure a good control of the beam-related background.

2 Requirements and challenges

To measure the number and energy spectrum of electrons and positrons per bunch crossing, challenges and requirements depend on two major scenarios. In the first, when the number of electrons and positrons is very small, the showers must be measured on top of low energy, but widely spread, background. In the second, when the number of electrons and positrons is large and single particle showers overlap, the number of electrons and positrons and their spectrum can still be measured using an energy flow algorithm as explained below. However, non-linearity of the readout electronics and potentially of the signal generation in the sensor has to be taken into account. In the first scenario, a small Molière radius and high granularity will improve the performance of the measurement. In the second, high granularity becomes essential.

The following studies are done for positrons, but they are valid also for electrons in the γ-laser setup. To get a quantitative picture, a custom-developed strong-field QED computer code, named PTARMIGAN [4], is used to simulate the strong field interactions for the relevant physics processes. Simulations are done for different laser parameters. For phase-0, at the start of the experiment, a laser power of 40 TW is assumed, while in phase-1 the laser power is increased to 350 TW. The positron yield per bunch crossing for e-laser and γ-laser interactions are shown in Fig. 2 as function of ξ, where ξ is the intensity parameter of the laser field. Different values of ξ are achieved by varying the laser. It is seen that for the e-laser mode the positron yield is larger than for the γ-laser

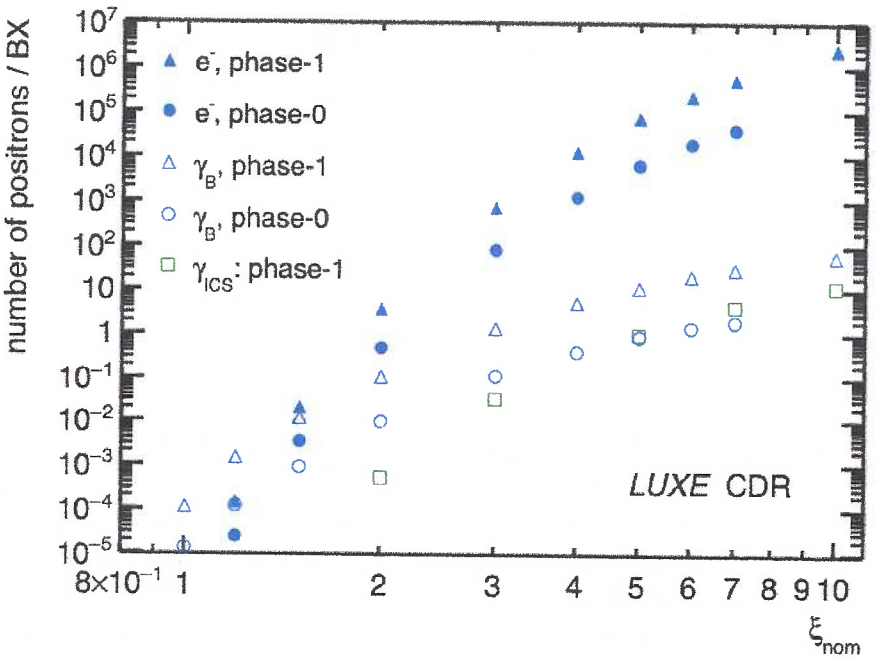

Figure 2: Number of positrons per bunch crossing produced in the e-laser and γ-laser setups for phase-0 and phase-1, as a function of ξ. The electron beam energy is set to 16.5 GeV, and the laser waist parameter varies between 100 μm and 3 μm in the range of ξ.

one by a factor of $\sim 10 - 10000$, depending on ξ. For phase-0 of the e-laser run, up to 10^5 positrons are expected per bunch crossing, while for the γ-laser running at low ξ, most of the bunch crossings are without a positron, and only $\sim 10^2$ are expected at the highest ξ. For phase-1 the rates are roughly 10–100 times larger.[1] The expected positron spectra are typically between 2 and 14 GeV, and are slightly softer for the e-laser mode, as can be seen in Fig. 3.

It would be interesting to compare with $\xi \ll 1$?

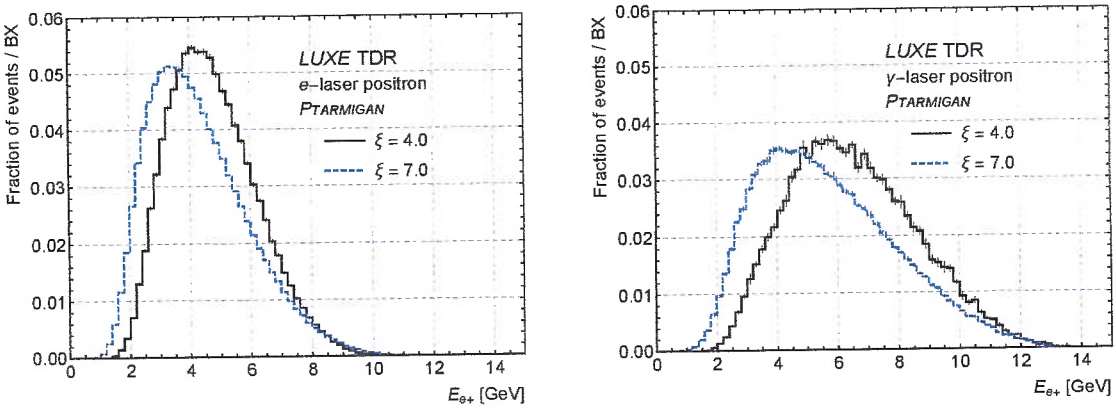

Figure 3: The positron energy spectrum for the e-laser and the γ-laser setup for phase-0 for different values of ξ.

Also shown in Fig. 3 are the expected energy spectra for phase-0 for both processes for selected ξ values. With increasing ξ values, the maximum of the spectrum slightly shifts toward lower energies. Why? Can one give any intuitive explanation ??

To keep the Molière radius small, a compact sandwich calorimeter with tungsten absorber plates interspersed with silicon pad sensors[2] is designed. The thickness of the tungsten plates is 3.5 mm, corresponding to one radiation length. The gap between two absorber plates is 1 mm, requiring firstly ultra-thin assembled detector planes, and secondly tungsten plates of very good flatness. The acceptance range in the horizontal, x, direction is defined by the positron spectrum and the magnetic field of the dipole magnet, and amounts to about 50 cm. The height in y direction is, due to the small Molière radius, only 5.5 cm.

For performance studies and layout optimisation, full detector simulations are performed using the GEANT4 package. Single positrons with different energies are generated by a gun for basic performance studies. For complex performance estimates, signal and background processes of e-laser and γ-laser interactions are generated with the precursor of PTARMIGAN, IPSTRONG [5].[3]

The ECAL-P is exposed to beam related background. For the electromagnetic component of the background, the expected particle rates and the energy sum of particles impacting

[1] These numbers can be reduced by defocusing the electron beam.

[2] Simulations are currently performed using silicon sensors of 320 μm. Currently sensors of 500 μm are froseen. The inpact of the results shown here is expected to be small.

[3] The differences between the two MC generators are mainly in the expected yields but not in the energy spectra and therefore the design of the ECAL-P did not have to be altered.

the calorimeter per bunch crossing as a function of the x position in the calorimeter are shown in Fig. 4 in the e-laser set-up for the phase-0 laser and $\xi = 3.1$. The background contribution is split into different particle types and compared to the expected yield of signal positrons.

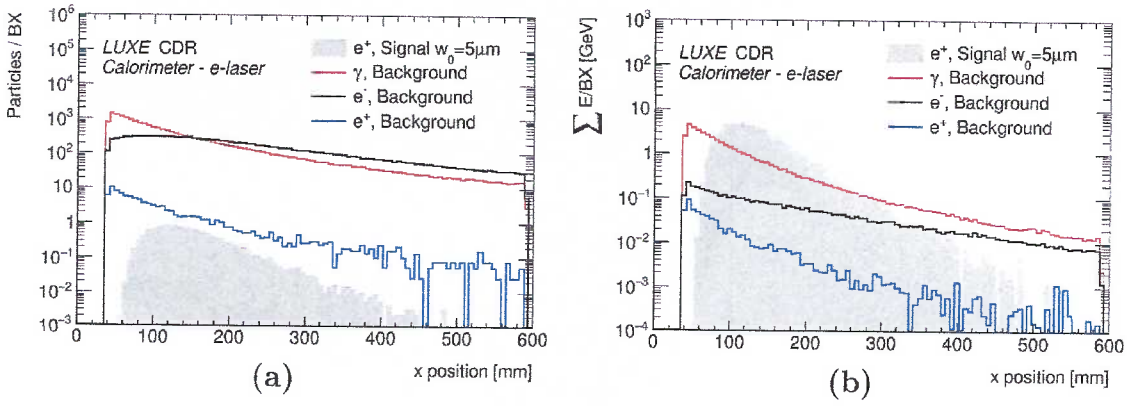

Figure 4: (a) Number of particles and (b) their energy sum per BX, split into different background particle types and signal positrons as described in the legend, as a function of the x position in the calorimeter for the e-laser set-up for phase-0 and $\xi = 3.1$.

Much of the background originates from a flux of very low energy secondary particles created by the beam, which will be further suppressed by optimisation of the vacuum chamber design, the shielding, and the beam-dumps. A new background source was recently identified, originating from the beam-dumps downstream of the ECAL-P, entering from the back of the ECAL. It consists of low energy neutrons. The effect of this background requires further studies with the FLUKA package, more adapted to this purpose, as well as optimisation of the beam-dumps design for low neutron back-scattering. Once these studies are completed, extra shielding behind the ECAL for which there is ample space will be considered. This is an ongoing effort. Finally, the irreducible background depositions constitute a signal offset which will be measured in bunch crossings without laser and subsequently subtracted from signal event depositions, pad by pad.

3 System Overview

The LUXE ECAL-P is designed as a sampling calorimeter longitudinally composed of 10 layers of 3.5 mm ($1X_0$) and 5 layers of 7 mm ($2X_0$) thick tungsten absorber plates, and assembled sensor planes placed in a 1 mm gap between absorber plates. The whole structure will be held by an aluminum frame, with slots on top to position the front-end boards (FEB). A sketch is shown in Fig. 5.
The ECAL-P is located 4.3 m from the interaction point (IP), 10 cm behind the tracker and 5 cm away from the beam-line on the side towards which the positrons are deflected. A 1 cm thick tungsten plate, extending along the beam-line from the exit of the vacuum chamber, will shield it from the side. The ECAL-P will be installed on a special optical table together with the tracker. From simulation and tests of the LumiCal

▽ This sketch shows 20×1 X_0 option.
I can prepare a similar one for 10×1 X_0 + 5×2 X_0 ...

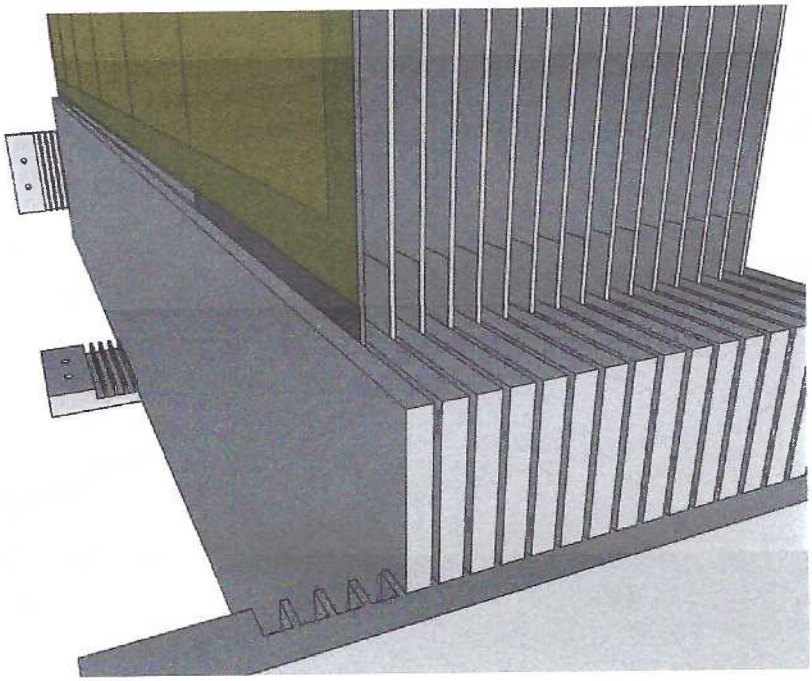

Figure 5: A sketch of the LUXE ECAL-P. The frame holds the tungsten absorber plates, interspersed with assembled sensor planes. The front-end electronics is to be positioned on top of ECAL-P and housed in a cage to avoid pick-up of electromagnetic noise.

prototype [2] on which the ECAL-P design is based, the expected energy resolution is $\sigma/E = 20\%/\sqrt{E/\,\mathrm{GeV}}$ and the position resolution is about 750 μm for electrons of 5 GeV[4]. The position resolution translates into $\sigma/E = 0.5\%$ to be compared to $\sigma/E = 9\%$ from calorimetry alone.

ECAL-P sensors are made of silicon wafers of 500 μm thickness. Each sensor has a surface of $89.8 \times 89.8\,\mathrm{cm}^2$ and consists of 256 pads of $5.5 \times 5.5\,\mathrm{mm}^2$ size (p on n-bulk type). Each complete detector plane will consist of 6 adjacent sensors. The fiducial volume of the calorimeter will then be $54 \times 9 \times 9\,\mathrm{cm}^3$.

The readout will be based on the FLAME multi-channel readout system [6, 7] which will be adapted for the needs of ECAL-P. The readout of the FEBs will be orchestrated by FPGA boards, connected with cables of a few meters length. The FPGA boards will be located in a rack near the ECAL-P. The FPGAs are connected to a computer via ethernet. The data acquisition and monitoring will be implemented in the EUDAQ system [8]. The power dissipation of the FEBs is estimated to be less than 1 W, hence no active cooling is needed.

For the γ-laser setup, ECAL-E, will be installed behind the tracker on the electron side, "symmetrically" to the ECAL-P. ECAL-E is a sandwich calorimeter with tungsten absorber plates of 2.1 and 4.2 mm thickness, adding up to $9.6X_0$, interspersed with 15 silicon sensors planes. The sensors are of the same structure as mentioned above, with pads directly connected to SKIROC2 ASICs [9], embedded inside the layer structure.

[4]These values are obtained when the positrons hit the calorimeter under a small angle due to deflection in the dipole magnet.

Figure 6: Left: picture of the 15 layer stack of ECAL-E. Visible are the mechanical housing the HV and LV cabling and the flat Kapton cable for the readout of the 15360 pads of the stack. Right: Zoom into the extremities of the stack to appreciate the compactness of the ensemble.

Four $9 \times 9\,\mathrm{cm}^2$ sensors form a sensor layer of 1024 pads, read out by 16 ASICs mounted onto a PCB. The 18×18 cm^2 sensor layer, assembled with ASICs, is called an Active Sensor Unit (ASU).
During 2021 and 2022 a stack with 15 ASUs, equivalent to 15360 readout channels, has been completed, as shown in Fig. 6.
The final ECAL-E will comprise three such stacks, to cover the full energy spectrum of electrons.

4 Expected performance

The performance of the ECAL-P was studied with the LUXE GEANT4 simulation assuming that a sensor plane consist of 320 μm thick silicon sensor, sandwiched between two Kapton layers supported by a thin carbon envelop, with the whole structure having a thickness of 830 μm. The sensors are subdivided in pads of $5 \times 5\,\mathrm{mm}^2$ area. For the current studies, the energy deposited in each pad is used. Signal sharing between pads and signal digitisation will be implemented in the future, based on the results of beam-tests.
In the following, we discuss the performance of the ECAL-P for single showers, with and without background, and the expected results for high rates of positrons where single showers cannot be identified and the spectrum is reconstructed through an energy-flow type of approach. The latter case is studied without background implementation. For the medium range rates, we are developing a clustering algorithm which should then lead to a performance similar to the one of single showers.

4.1 Energy and Position Resolution for single positrons

The performance of the ECAL-P for single positrons was studied by generating samples of positrons in the energy (E_0) range between 2 and 15 GeV in steps of 0.5 GeV, assuming the positrons originated from the IP. The positrons enter the calorimeter at an angle due to the deflection in the dipole magnet. After calibration, which takes into account the angular dependence of the response, the dependence of the relative resolution σ/E as a function of the initial positron energy is shown in Fig. 7. A fit of the form $\sim 1/\sqrt{E_0}$ leads to

$$\frac{\sigma_E}{E} = \frac{(20.2 \pm 0.1)\%}{\sqrt{E_0/\mathrm{GeV}}} \,. \tag{1}$$

For the position reconstruction, a logarithmic weighting of the energy deposits in the pads is applied, with a threshold optimised to give the best resolution. Along the y-axis, not affected by the deflection in the dipole magnet, a resolution of $\sigma_y = 460\,\mu$m is achieved. Along the x-axis, $\sigma_x = 550\,\mu$m at 10 GeV is obtained, and a mild dependence on the energy is found. However, while along the y-axis no bias in the position reconstruction is observed, this is not the case for the x position. As shown in Fig. 7, for positrons of 10 GeV, a bias of $\delta x \simeq 500\,\mu$m is generated by the fact that the positrons impact the ECAL-P under a small angle. This is not critical as this bias can be corrected for. An approach based on convoluted neural networks was also applied to the position reconstruction. The resolution (not shown) was not better than for the logarithmic weighting, however there was no bias in the results. The alternative method of determining the energy for single

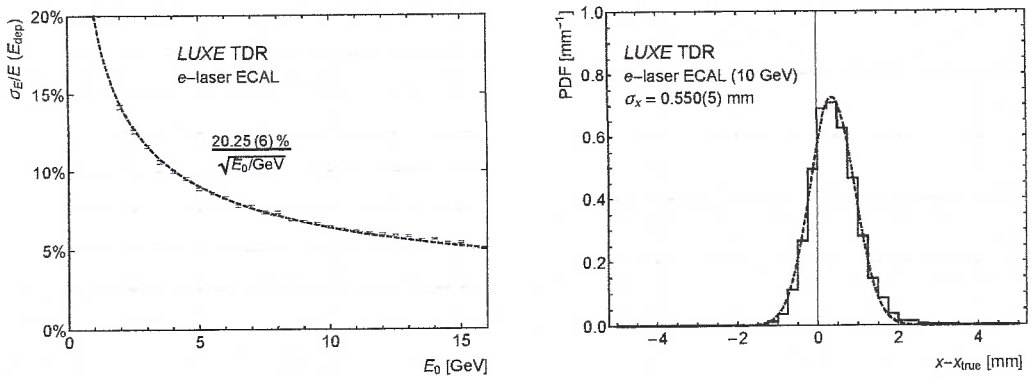

Figure 7: Left: The relative energy resolution of the ECAL-P as a function of the positron energy. Right: The difference between the reconstructed and the generated entry point of the positron shower along the magnetic deflection (x) axis for 10 GeV positrons.

positron showers is by making use of the correlation between energy and position of the positron entry point on the face of the ECAL. The relative energy resolution is then determined by the position resolution. The position resolution as a function of positron energy is shown in Fig. 8. Also shown in the figure is the resulting σ/E compared to the one from calorimetry shown in Fig. 7. Not surprisingly, the σ/E from position reconstruction is better by factor 10 (high energy) to better than 40 (low energy) in the relevant energy range.

This line does not correspond to the fit shown in the left figure. This should be corrected...

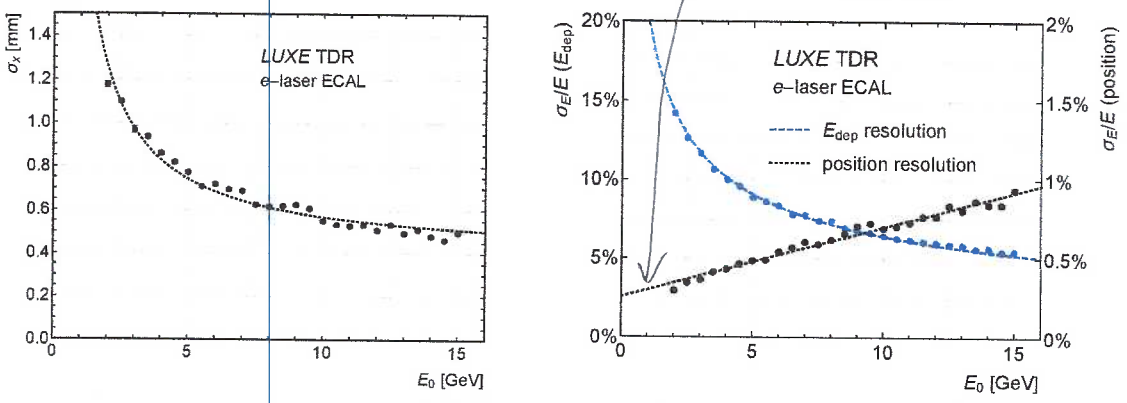

Figure 8: Left: Position resolution as a function of positron energy. Right: The relative energy resolution of the ECAL-P as a function of the positron energy from position reconstruction (right y-scale) compared to the relative resolution from calorimetry (left y-scale). ← Is it the same curve as in Fig 7.? It should be mentioned.

4.2 Impact of background

It is important to ensure that this performance can also be achieved in the presence of background which is particularly sizeable near the beam-line. In this section, we only consider the electromagnetic component of the background. The hadronic component is still under study. The distribution of the background depositions per e-laser bunch crossing is shown in Fig. 9. Also shown in the figure are the depositions for a single positron of 5 GeV. The depositions of the single positron are in a small cone around the

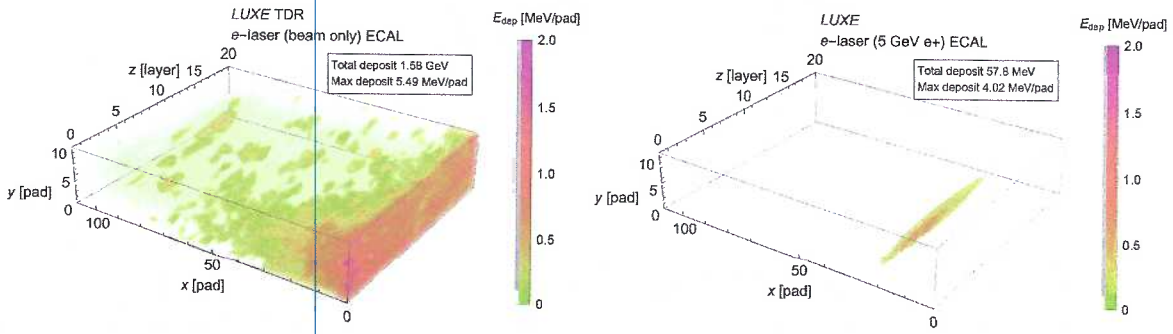

Figure 9: Left: Depositions per bunch-crossing from beam-related background inside the ECAL-P. The beam-pipe is located on the right side. Right: Depositions from a positron of 5 GeV.

shower axis. The background is widely spread and its contribution increases towards the beam-pipe. The effect of this background on the energy deposited in the cone around the shower axis is shown in Fig. 10 for several positron energies. The distribution of the energy deposited by positrons of a given energy is compared to the distribution obtained after adding the background to all pads containing the electromagnetic shower. One clearly observes a shift in the total deposited energy but no significant deterioration in

- Do you include background fluctuations ?? It does not make any sense just to add average bg level...
- Pad selection / clustering is crucial! Is it modelled?

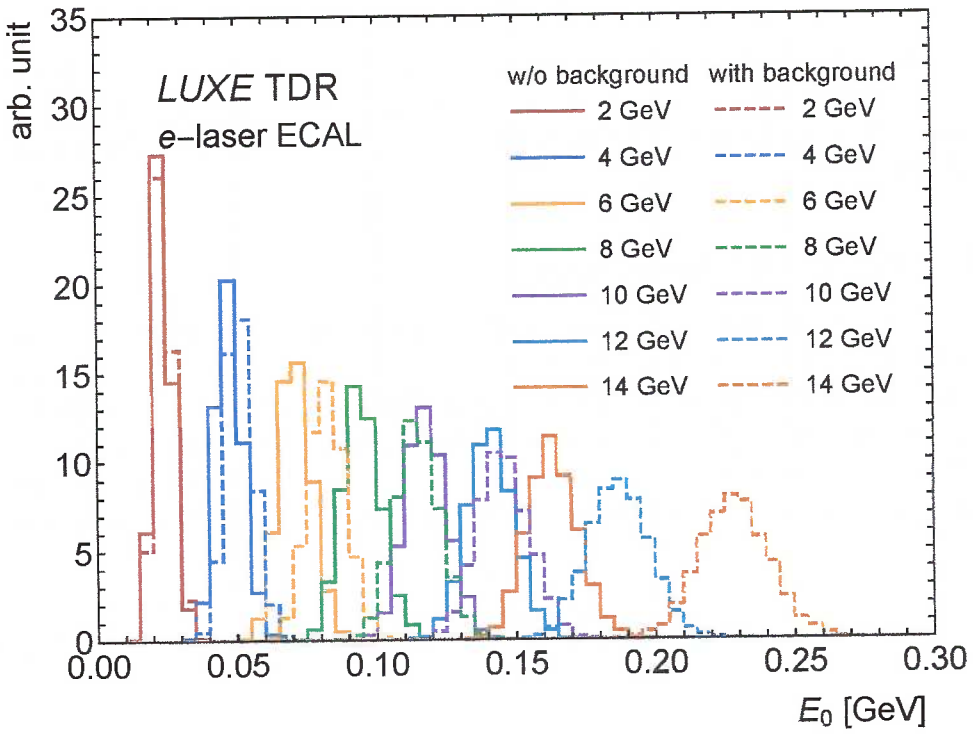

Figure 10: Distribution of total energy deposited in the sensor-pads of the ECAL-P for selected energies of positrons (full lines) and for the same positron showers with added background (dashed-lines) in the e-laser setup. The various energies of the positrons listed in the legend are identified by different colours.

the resolution. As expected, the shift in energy is the more pronounced the higher the energy of the positron, the closer it gets to the beam-line. This is illustrated in Fig. 11 where the ratio between the expected energy deposition with and without background is shown as a function of the positron energy for the e-laser setup. The present estimate of the background contribution is higher than the estimate presented in the CDR (also shown in the figure) because of the change in the window-material at the exit of the vacuum chamber. In the most up to date experimental setup the exit window is made out of aluminium as opposed to Kapton used in the CDR simulations. The expected shift in

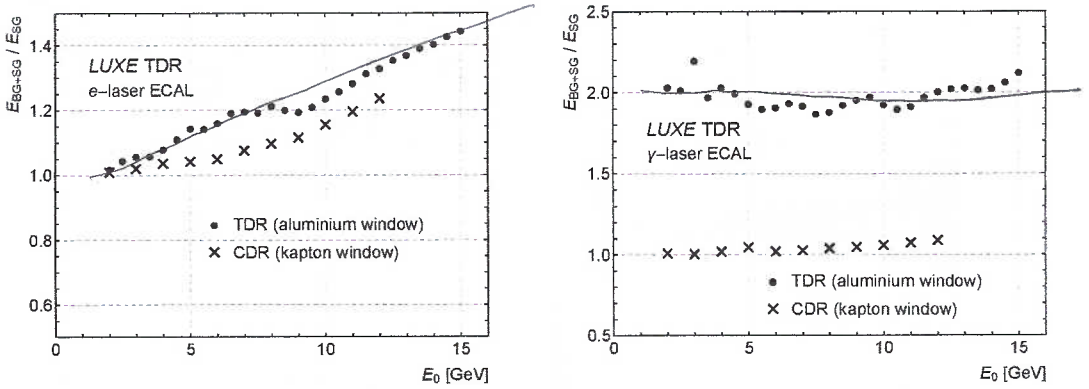

Figure 11: Ratio of the expected energy deposition in the ECAL-P with background to the one without background as a function of positron energy. (Left) e-laser setup for the aluminium exit-window (TDR) and the Kapton window (CDR), with only electromagnetic background. (Right) γ-laser setup for the Kapton window (CDR) with only electromagnetic background and for the aluminium window with hadronic background included.

the deposited energy for the γ-laser setup due to electromagnetic background is smaller than in the case of the e-laser setup for the same window type, due to smaller background level, as shown in Fig. 11. For the aluminium window, when the hadronic background is included without extra shielding for the beam-dump, the ratio of signal with background to signal alone increases by almost a factor two. If the observed shift in the energy deposited in the ECAL-P due to background remains after extra shielding against neutrons at the level shown in Fig. 11, it will be corrected for by direct background measurements with electron or photon bunches crossing the detector without interaction with a laser pulse. The effect of the background on the resolution of the ECAL-P is small for most of the fiducial volume.

4.3 Reconstruction of Positron Number and Spectrum

When the number of positrons entering the ECAL-P becomes large, the showers start overlapping and it becomes impossible to identify individual clusters. Instead a method based on energy-flow is proposed [10], whereby each pad contributes a fraction of the number of positrons in a given energy bin. The latter is determined from the crossing of the path connecting the centre of the pad to the IP, according to the dipole magnet field

and the geometry, with the face of the ECAL-P, as if the pad was located on the axis of the shower generated by the impinging positron. At the end of this procedure, both the energy spectrum observed in the ECAL-P and the number of positrons (sum over all energy bins) are reconstructed. An overall correction of the order of 2% has to be applied to the reconstructed number of positrons to obtain the number of generated positrons. The relative spread of the number of reconstructed positrons as a function of the number of incident positrons is shown in Fig. 12 (Left). For an average positron multiplicity of about 1000 the projection on the vertical axis is shown in Fig. 12 (Right) . The uncertainty is less than 0.5%. The comparison between the generated and reconstructed

? It looks like close to 0.5% from the figure

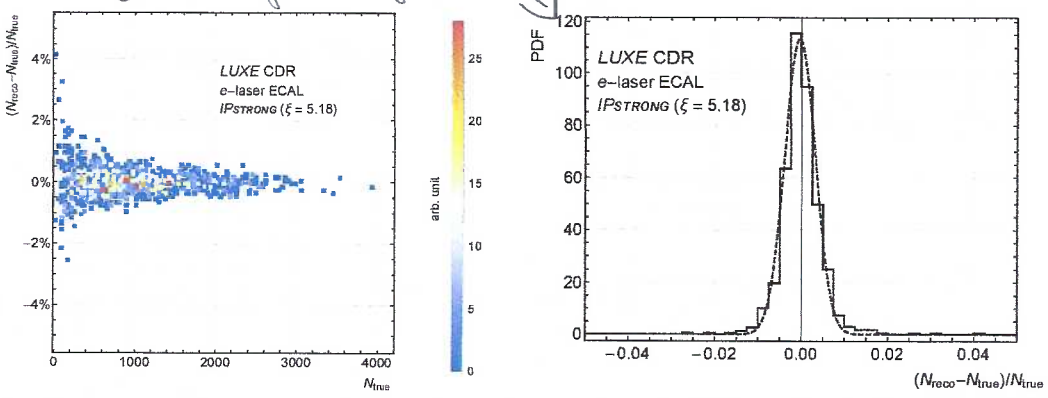

Figure 12: Left: The relative spread of the number of reconstructed positrons as a function of the number of incident positrons. Right: Projection of the relative spread onto the vertical axis for a average positron multiplicity of 1000.

energy spectra is shown in Fig. 13. A good agreement between the two spectra is found, with the exception of the low-energy and high-energy tails, where leakage of the showers sets in. The same reconstruction method was applied to multiplicities of the order of 10^5 (not shown) and still reasonable agreement was found, though the overall correction factor increased to 5%. However, positron multiplicities of this order very likely cannot be measured by the ECAL-P, as they would lead to distortions in the charge drift due high charge density in the sensor and to saturation of the FE ASICs. This problem is under study in order to determine the highest positron multiplicity that can be handled by the ECAL-P. Changing the bunch charge or the electron beam width allows at very large ξ to reduce the number of positrons such that it matches the dynamic range of ECAL-P. Studies to implement image recognition with convoluted neural networks for the reconstruction of the energy spectra and multiplicities is under investigation. It turns out that with the first 10 layers of the ECAL-P one can already derive the positron multiplicity and the average energy on an event by event basis. Further studies are underway to reconstruct the full energy spectrum.

The ECAL-E has been introduced only recently into the geometry of LUXE and the study of its performance is underway. However given the similarity between the ECAL-P and ECAL-E in sampling and granularity, similar results are expected.

/

fraction?

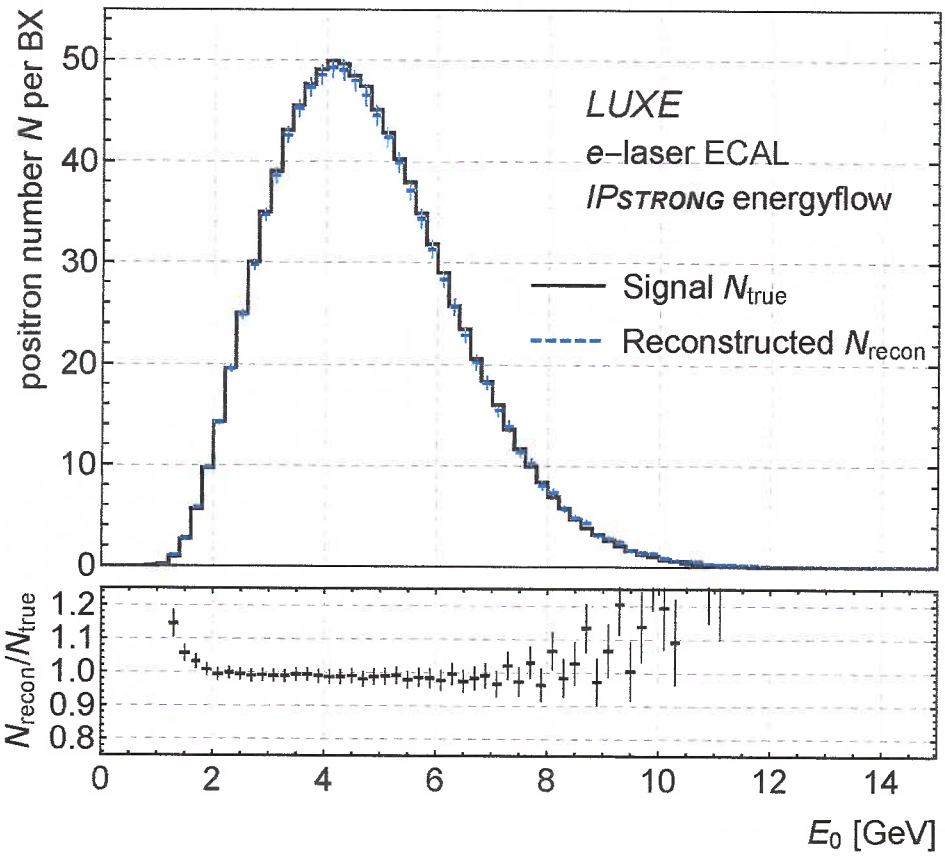

Figure 13: Comparison between the reconstructed and generated energy spectra of the positrons. The ratio of the two spectra as a function of energy is displayed in the lower panel.

Some description of the case should be included as in Fig 12
(For average positron multiplicity of 1000)

5 Technical description

In the following subsections the mechanical structure, the sensors, the structure of the sensor planes, the front-end (FE) electronics and the data acquisition of ECAL-P are described in detail.

5.1 Mechanical Frame and Tungsten Plates

Frames made of aluminium ensure the mechanical stability of the calorimeters and allow the precise positioning of sensor planes and tungsten plates. The frame of ECAL-E will be designed and constructed by the University of Warsaw. A sketch of the frame with some inserted tungsten plates is shown in Fig. 14.

ECAL-P ?

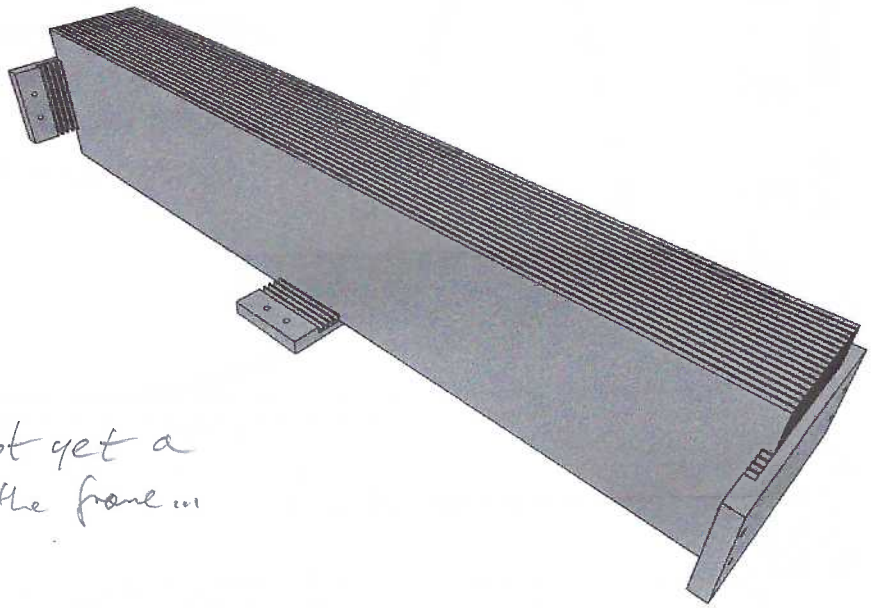

This is not yet a sketch of the frame...

Figure 14: The mechanical frame of ECAL-P with several tungsten plates inserted. The frame is made of aluminium.

The requirement on the mechanical frame is to allow the insertion of 10 tungsten plates of dimensions $560 \times 90 \times 3.5\,\mathrm{mm}^3$, and 5 tungsten plates of dimensions $560 \times 90 \times 7\,\mathrm{mm}^3$ parallel to each other with a gap in-between each two plates equal to 1 mm, with a maximal deviation of $\pm 100\mu$m all over the tungsten plate surface. All materials used must be non-magnetic. The 15 tungsten plates will be moved in very precise aluminium combs, ensuring that the distance in-between plates is equal to the reference distance within $\pm 100\mu$m. The mechanical frame of ECAL-P will be designed and constructed in the IJC lab in Paris. The requirements on precision are the same as given above for the ECAL-P.

ECAL-E ?

This should not be considered fixed yet!
Some space is needed for carbon fibre envelope frame.
I would add $\gtrsim 2 \times 2$ cm to the sensor size (54 cm)
so it should be at least 58 cm
Also the width should be slightly longer than sensor size ($\gtrsim 10$ cm)

5.2 Sensors

The silicon sensors, used both for ECAL-E and ECAL-P, are arrays of $5.5 \times 5.5\,\mathrm{mm}^2$, $p+$ on n substrate diodes made of $500\,\mu\mathrm{m}$ thick silicon with a resistivity of $3\,\mathrm{k}\Omega\mathrm{cm}$, and a reverse bias voltage of about 200 V, without guard rings. Each sensor will have a total area of $89.7 \times 89.7\,\mathrm{mm}^2$, corresponding to 16×16 pads. Sensors of area $89.7 \times 89.7\,\mathrm{mm}^2$ have been produced by Hamamatsu Photonics for the CALICE Collaboration, as shown in Fig. 15, and four of them were tested for LUXE purposes.

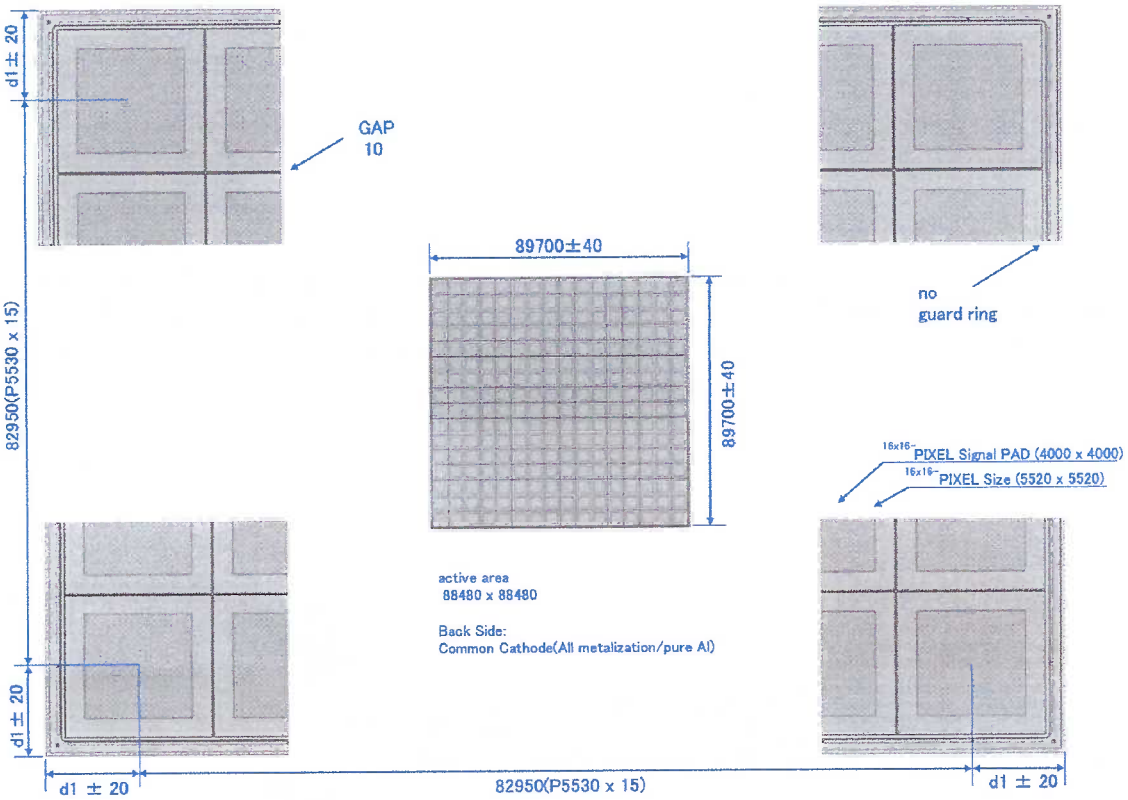

Figure 15: Details of the geometry of the CALICE sensor.

For all pads of the four sensors the leakage current was measured as a function of the bias voltage. A typical result is shown in Fig. 16. In order to route the signal from the pads to the front end board, a flexible PCB has been designed. It will be glued on the silicon sensors with a conductive glue. Another flexible PCB has been produced to connect the bias voltage to the sensor back-plane.

5.3 Assembled Detector Plane

In ECAL-E, signals from the sensor pads are routed to the FE electronics via copper traces on a flexible Kapton foil of $120\,\mu\mathrm{m}$ thickness. Conductive glue will be used to connect

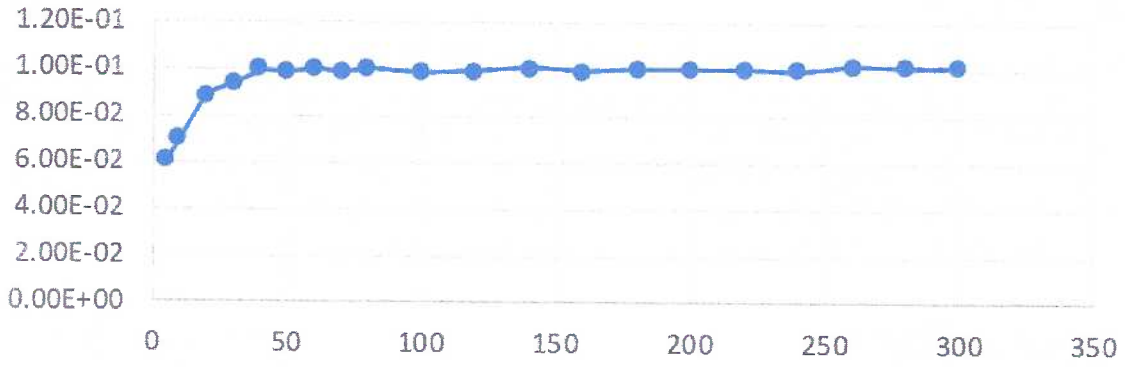

Figure 16: Leakage current (in nA) as a function of the applied voltage (in V) for a selected CALICE pad.

the copper traces to the sensor pads. The bias voltage is supplied to the back-side of the sensor by a 70 μm flexible Kapton-copper foil, glued to the sensor with a conductive glue. A sketch of the structure of the detector plane using a Kapton fanout is shown in Fig. 17. A carbon fiber layer is used to protect the sensor.

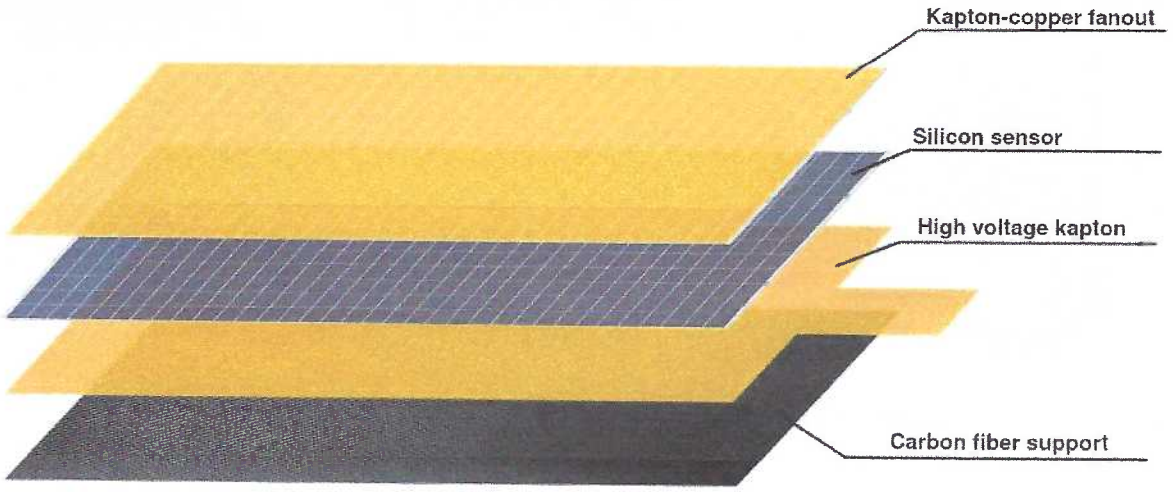

Figure 17: The structure of the assembled detector plane using a Kapton fan-out for the signal routing. The total thickness of the plane is about 830 μm.

5.4 Front-end electronics

In ECAL-P, each detector plane will be read out by FE ASICs called FLAXE (**F**ca**L** **A**sic for **X**FEL **E**xperiment), mounted on a PCB, denoted hereafter as front-end board, FEB, and positioned on top of the calorimeter frame. On the side of the FEBs, connectors are foreseen for cables to transfer digital signals from FLAXE ASICs to the FPGAs installed at a larger distance. The FLAXE FE electronics is based on the existing readout ASIC

called FLAME (**FcaL** Asic for Multiplane r**E**adout), designed for silicon-pad detectors of the LumiCal calorimeter for a future electron-positron linear collider experiment. The main specifications of the FLAME ASIC are shown in Table 1. A block diagram of

Variable	Specification
Technology	TSMC CMOS 130 nm
Channels per ASIC	32
Power dissipation/channel	$\sim 2\ mW$
Noise	$\sim$1000 e^-@10 pF + 50e^-/pF
Dynamic range	Input charge up to $\sim 6pC$
Linearity	Within 5% over dynamic range
Pulse shape	T_{peak} ~55 ns
ADC bits	10 bits
ADC sampling rate	up to $\sim 20\ MSps$
Calibration modes	Analogue test pulses, digital data loading
Output serialiser	serial Gb-link, up to 9 GBit/s
Slow controls interface	I^2C, interface single-ended

Table 1: Summary of the specifications of the FLAME ASIC.

FLAME, a 32-channel ASIC designed in TSMC CMOS 130 nm technology, is shown in Fig. 18. FLAME comprises an analog front-end and a 10-bit ADC in each channel, followed by a fast data serialiser. It extracts, filters and digitises analogue signals from the sensor, performs fast serialisation and transmits serial output data. As seen in Fig. 18,

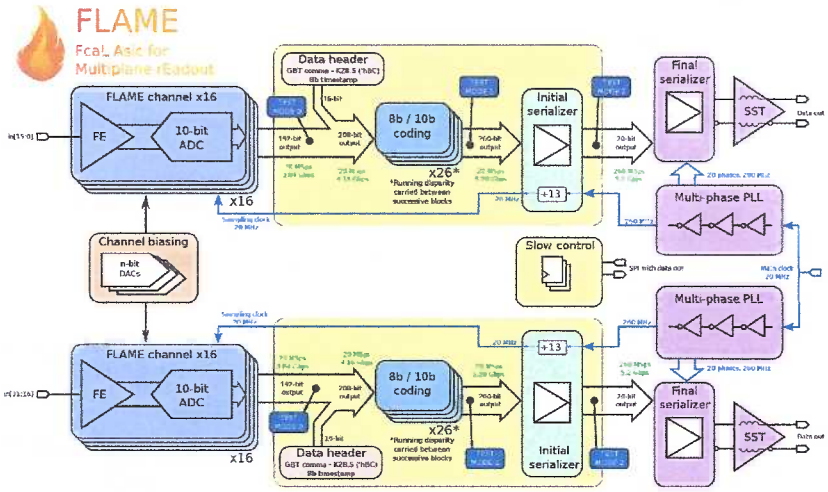

Figure 18: Block diagram of a 32-channel FLAME ASIC

the 32-channel chip is designed as a pair of two identical 16-channel blocks. Each block has its own serializer and data transmitter so that during operation two fast data streams are continuously sent to an external data acquisition system (DAQ). The biasing circuitry

is common to the two 16-channel blocks and is placed in between. Also the slow control block is common and only one in the chip. The analogue front-end consists of a variable gain preamplifier with pole-zero cancellation (PZC) and a fully differential CR–RC shaper with peaking time ~ 55 ns. The shaper includes also an 8-bit DAC, with 32 mV range, for precise baseline setting. The analogue front-end consumes in total $1-1.5$ mW/channel. The ADC digitises with 10-bit resolution and at least 20 MSps sampling rate. The power consumption is below 0.5 mW per channel at 20 MSps. In order to ensure the linearity of the ADC, the input switches are bootstrapped, reducing significantly their dynamic resistance.

The architecture of the FLAXE ASIC will be very similar to the existing FLAME design. In particular the same analog signal processing scheme will be kept. A few modifications are needed, mainly in the digital part. The fast data transmission components will be replaced by a simpler and slower data transmitter to reduce the complexity and the cost of the subsequent FPGA-based back-end and DAQ system. This is possible, since the data rate and data volume in LUXE is much less than for LumiCal. Depending on the sensor type which will be used in the experiment, small adjustments in analog front-end, e.g. charge-to-voltage gain, may also be needed. The dynamic range of the ASICs can be switched between high and low gain. At high gain the response to the input charge is almost linear between deposition from 0.5 to 75 minimum-ionising-particle (MIP) equivalent. At low gain the charge at the preamplifier input is limited to 5 pC, corresponding to about 10000 MIP-equivalent, and the lower threshold is in the range of a few 10 MIP-equivalent.

The power dissipation of the FE electronics amounts to a maximum value of about 50 W. However, it can be reduced by roughly a factor 10^3 by power pulsing, foreseen for application in LUXE. Hence for normal operation, cooling will not be needed. However, for calibration and alignment it is planned to take data with cosmic muons. For this case dedicated air cooling of the FEBs will be foreseen.

In ECAL-E, SKIROC2 ASICs, integrated in the sensor plane, are used. A picture of an assembled sensor plane is shown in Fig. 19. The main specifications of the SKIROC2 ASIC are shown in Table 2.

Variable	Specification
Technology	AMS SiGe 350 nm
Channels per ASIC	64
Power dissipation/channel	$\sim 6.2\ mW$
Dynamic range	Input charge up to $\sim 10pC$ high and low gain
Linearity	Within 1% over dynamic range
Pulse shape	T_{peak} 30-120 ns, tunable
ADC and TDC bits	12 bits

Table 2: Summary of the specifications of the SKIROC2 ASIC.

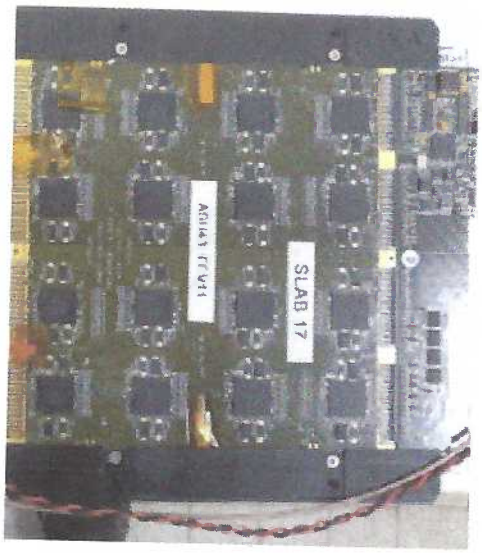

Figure 19: A fully instrumented sensor plane for ECAL-E. The SKIROC2 ASICs are positioned of the silicon pad sensor

6 Interfaces and Integration

6.1 Trigger

For the normal operation of ECAL-E and ECAL-P, the trigger will be provided by the Trigger Logic Unit (TLU), as shown in Fig. 20 and described in detail in the LUXE DAQ technical note [11].

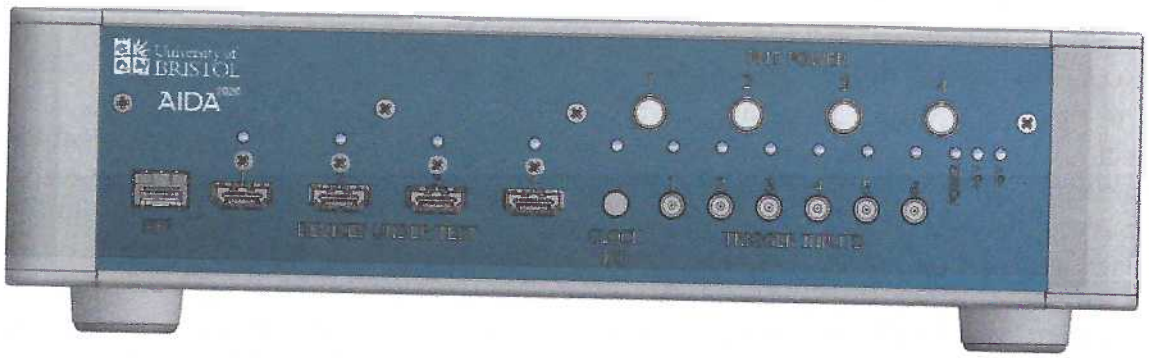

Figure 20: Front view of the TLU.

The TLU will distribute to all the sub-detectors the trigger signal coming from

- the electron beam with a frequency of 10 Hz,
- the laser beam with a frequency of 1 Hz.

In ECAL-P, the trigger signal will be sent to the FPGA-based back-end, which will then distribute it to the FLAXE ASICs located at the FEBs via dedicated differential links. The FPGA will perform a programmable phase shift of the trigger signal in order to wake up the FLAXE ASICs just before the next bunch crossing using the power pulsing feature. Effectively, the FPGA will use the trigger originating from a particular bunch crossing to predict the next one, to start the analogue and the mixed-mode signal processing, as well as the data acquisition in the FLAXE ASICs. The ASICs will remain active, writing the data into an internal memory, in a time window sufficient to fully collect the bunch crossing event. After this time, the analogue and mixed-mode signal processing part of the FLAXE ASICs will be automatically switched off, and data collection will be stopped. The collected event will be held in the internal FLAXE ASICs memory and successively read out by the FPGA between bunch crossings.
During the construction of the ECAL-P at DESY, a cosmic muon trigger will be installed. It will consist of two scintillators and PMTs, connected to NIM modules to create the logic. This will provide an asynchronous trigger to the FPGA-based back-end, which will be distributed the same way as the synchronous trigger, only without the phase shift. The FLAXE ASICs will run continuously, processing and collecting the data into the circular buffer in the internal memory integrated into the ASICs. The asynchronous trigger will then stop the data collection in the ASICs, allowing the FPGA to read out the cosmic muon event. The data collecting process will restart automatically as soon as the event data is read out by the FPGA.

6.2 Data Acquisition

In ECAL-P, the six silicon detector planes in each ECAL-P layer will be equipped with a single FEB, common for all sensors in the layer. All FLAXE ASICs on a FEB will be connected in parallel to the common data bus. The data bus will use a SPI-like, synchronous, serial protocol in the physical layer, with three differential links for the bus clock, a serial CLock, SCLK in the range $20 - 60$ MHz. Commands are send from FPGA to the ASIC in the regime 'Master Output'–'Slave Input', MOSI, and data from ASIC to the FPGA as 'Master In'–'Slave Output', MISO. However, in the logical layer, the bus will implement a I2C-like protocol, allowing the FPGA to address and communicate with each ASIC independently. The event data from a single ECAL-P layer will be read out from the FLAXE ASICs sequentially, one ASIC after the other. This bus, on top of the data acquisition, will also serve the slow control and the configuration interface to the ASICs.
Up to 128 raw ADC samples will be collected in an event for each of the readout channels. With about 1000 channels per single ECAL-P layer and a 10 bit ADC resolution the event size amounts up to 1 Mb. With 10 Hz of bunch crossing rate, this results in about 10 Mb of data per second read out from a single FEB. Therefore the 20 MHz bus clock frequency provides a sufficient bandwidth for a regular operation. A higher bus clock frequency is foreseen for the data acquisition of the asynchronous muon calibration mode, in order to reduce the dead time of the system.
The data from each FEB will be sent to the FPGA board. Since only three, relatively slow, differential links are needed for a single FEB, the data of the whole ECAL-P can be

read out and processed by a single FPGA. The signals from the FEBs are fully digital, hence the FPGA board can be positioned at a larger distance from the calorimeter, e.g. in the calorimeter rack. The FEBs will be read out in parallel via different links. Hence, the bandwidth which is sufficient to read out a single FEB will also be sufficient to read the whole ECAL-P between consecutive bunch crossings.
The event will be processed by the FPGA. The signal reconstruction comprises the calculation of the deposited charge and the Time Of Arrival, TOA, from the collection of the raw ADC samples in a given channel. This procedure, combined with zero suppression, will significantly reduce the data rate. Finally the remaining event data will be sent from the FPGA board to the DAQ computer using the User Datagram Protocol, UDP, through a single 1 Gbps Ethernet link. In parallel, the Transmission Control Protocol, TCP, over the same link will be used for the system control and monitoring.

7 Installation, commissioning and calibration

7.1 Detector assembly

The ECAL-E will be fully assembled and tested at LAL Orsay and shipped to DESY. After arrival a system test will be performed and the status of all components will be documented. The time foreseen is two weeks.
The ECAL-P assembly requires the presence of participants from four institutes engaged in building the ECAL-P:

- UW - for the mechanical frame and the tungsten plates.
- TAU - for installing the sensor planes between the tungsten plates.
- AGH-UST - for installing the readout electronics.
- ISS - for software support and slow control.

The assembly will take place at DESY.
The tasks to be performed are then

- Inserting the tungsten plates, plate by plate, and the sensor planes in between.
- Connecting the FEBs and the electronics.
- Performing a cosmic run for function tests of components.

Sensor planes need to be connected to FEB before assembly!!

It is assumed that it will take a day to install one tungsten plate and one sensor plane, and perform the function tests. The tungsten plate will be inserted into the mechanical frame followed by cabling and connection of FEBs, HV and LV as well as DAQ. After performing a noise check, data from cosmics will be collected during the night. This cycle will be repeated for the 15 plates. It will thus take 15 days to complete these tasks. This will be followed by a full system test for about 5 days. Another 10 days will be needed to perform the ECAL-P calibration in the DESY test-beam. The full assembly is thus expected to take about a month. With an added contingency to solve unforeseen

This procedure does not make sence if sensor planes are independent. One should first assemby all tungsten plane. Then check the structure, gap sizes (with a dummy sensor plane (or dedicated measurement module). Only then assembly sensors ...

problems, the total time estimate for ECAL-P readiness to be moved into the experiment is thus 1.5 months.
During the phase of the construction of the ECAL-P, the DAQ should be able to work in a standalone mode with a cosmic trigger. For the latter, two scintillators with PMTs and one NIM crate with a trigger based on NIM modules will be provided. Once the ECAL-P is fully tested, the whole system is moved to the pit and the DAQ PC of ECAL-P will be included in the central LUXE DAQ.

7.2 Installation

For the final installation in the experimental area, it is assumed that:

- the table on which the ECAL-E and ECAL-P is placed is installed;
- all LV, HV and data cables are installed to connect the ECAL-E and ECAL-P subsystems with the rack.

The installation steps, with the estimated duration and the number of participants, are as follows:

- Moving the ECAL-E and ECAL-P to the area and place it on the table. The rough weight estimate is 50 kg and thus a crane will be needed.
  Duration: 1 day;
  Person power: 1 technician (DESY), 2 physicists for ECAL-E and ECAL-P each.
- Moving the electronics racks to the area next to the ECAL-E and ECAL-P (time and person-power included in the previous item).
- Performing the survey, to precisely define the position of ECAL-E and ECAL-P;
  Duration: 1/2 day;
  Person-power: experts from DESY/XFEL survey, 1 physicist for ECAL-E and ECAL-P each.
- Connecting the cables between ECAL-E and ECAL-P and the rack.
  Duration: 1 day;
  Person power: 1 electronic engineer, 1 technician, 1 physicist ECAL-E and ECAL-P each.
- Testing of HV, LV and data connections. Duration: 1 day plus 2 days in reserve for potential replacements;
  Person-power: 1 electronics engineer, 2 physicists ECAL-E and ECAL-P each.

Hence for the installation of the ECAL-E and ECAL-P in the area between 3.5 to 5 days are needed for each of them. The process will be performed by 2 physicists, 1 electronic engineer and 1 technician (partly provided by DESY), and the DESY survey team. A summary is given in the resource loaded schedule in appendix A.

7.3 Commissioning

After installation, the full system test will be repeated. Low voltage settings and currents drawn by the sensors and the FE ASICs will be checked. Pedestal data will be collected with a special trigger, and the pedestal values and width monitored, as a proof of stability and readiness for operation.

7.4 Calibration Strategy

The ECALs will be calibrated in electron beams of precisely known energy. The electron-beam energy available at DESY is limited to 6 GeV. The positron/electron energy range expected in LUXE for Breit-Wheeler type of processes extends to about 15 GeV. Therefore beam-tests at CERN will be required.

To save time and minimise the risks of mechanical damage to the ECAL-P, the following strategy will be adopted. The existing FCAL tungsten prototype mechanical structure will be equipped with 20 sensor planes and FLAXE readout boards. It will then be tested and calibrated in the DESY and CERN test-beams. This will allow to develop the proper MC simulation with digitisation within GEANT4. The full ECAL-P will be exposed to the DESY test-beam and the comparison between the results obtained with the FCAL prototype and the ECAL-P at low electron energy will then be used to project the performance of the full ECAL-P at higher electron beam energies. This approach provides more flexibility in the access to test-beams.

Tuning of the calibration after installation will be done in special runs foreseen in LUXE using a photon beam. A needle will be inserted near the IP to convert photons to electron-positron pairs. These pairs will be used to calibrate the tracker energy by imposing the constraint that the invariant mass of the pair has to be zero. The "calibrated" tracks will then be used to cross-calibrate the ECALs. The expected energy resolution of the tracker is within factor two the same as the one of the calorimeter when deduced from the electron or positron position reconstruction.

7.5 Decommissioning

The decommissioning of the ECALs will be done by the laboratories having developed and built the ECALs, as listed in Table 5. The decision about a potential further use of ECAL-E or ECAL-P, or its dismantling, will be decided by the involved parties before the completion of the LUXE the experiment. In case of dismantling, each laboratory will take back the delivered components. The time needed for decommissioning depends on a potential activation of the material, e.g. near the beam line. About a potential intermediate storage at DESY, the parties will propose an agreement with DESY.

8 ORAMS: Operability, Reliability, Availability , Maintainability and Safety

The number of readout channels of ECAL-P and ECAL-E is about 25000, orchestrated by FPGAs. Since the readout frequency during normal data taking is 10 Hz, there should

For ECAL-P it is equivalent with replacement of the sensor plane!

be no problem with the speed of readout and data transfer. The radiation dose for sensors and FE electronics is below a critical level, hence radiation damage is not expected. Solid state sensors are devices of high reliability. There will be no danger of over-voltage breakthrough or sparks. The change of the leakage current due to temperature changes will be kept small by air conditioning in the area, with a maximum temperature drift of a few °C. The ECAL-P and ECAL-E are modular. In case of malfunctioning of a detector plane it can be replaced by a spare part within a few days of access. For the replacement of faulty FE ASICs or FPGAs, less than a day will be needed. The same holds for the Low Voltage and High Voltage power supplies. The bias voltage for the sensors will be around 100 V. High Voltage connectors and cables will be used, matching the safety requirements.

9 Project Organisation

University of Warsaw! (this is the official name)

9.1 Human and financial resources

ECAL-E and ECAL-P will be built in a joint effort of the AGH-University of Technology (AGH-UST) Cracow, the Kyushu University (KU), the Laboratoire de Physique des 2 Infinis Irène Joliot-Curie, (IJC) Paris, the Laboratoire Leprince-Ringuet (LLR) Paris, the Institute of Space Science (ISS) Bucharest, the Tel Aviv University (TAU), the Universitat de Valencia (IFIC) and the Warsaw University (UW). These institutes will provide the human and financial resources needed for the design, production, test, commissioning and operation of ECAL-P. The group of AGH-UST comprises 5 experienced researchers, specialised in ASIC design, 1 technician and several students. From the Kyushu University one researcher specialised on sensors will join, the Laboratoire -Ringuet Paris will contribute with mechanics, sensor assembly and electronics of ECAL-E with 2 researchers. From the ISS group, 3 physicists experienced in software and data handling are included. The TAU group comprises 3 experienced physicists, 1 part-time technician (full time technician will be hired in the near future), one postdoc, and several under-graduate students. In the Universitat de Valencia one experienced researcher and one Ph.D. student will perform the gluing, and the Warsaw University with 2 experienced researchers, one Postdoc and engineering support design and build the mechanical frame of ECAL-P.

still not sure. Also, we have a candidate but we do not have money... (yet)

The cost estimate for the production of ECAL-P is given in Table 3. The major cost drivers are the sensors and the FE ASICs. TAU will cover half of the sensor costs, and received support from the PAZI Foundation (Israel Atomic Energy Commission) and has applied for support from the Israel Science Foundation. For the other half of the sensor costs the labs in the table above will make a joint application to their funding agencies. Compared to the CDR, the estimated price of FE ASICs has increased by about 25% mainly due to expected increased production costs. To cover the costs of the FE ASICs the AGH-UST group has successfully applied for a grant from the Polish National Science Centre, covering again about half the costs.

To cover the costs for the mechanics the UW will apply for support from the national funding agency. Costs for tungsten plates of precise thickness and flatness will be shard between LLR and TAU. The DAQ will be partly funded from the AGH-UST application. IJC and LLR will apply for additional funding. PCBs, power supplies, tooling and auxiliary components will be shared between AGH-UST, TAU and IJC. IFIC will apply for

Table 3: Cost estimates for the various components. The comment discusses the source of the price and its uncertainty where possible.

Component	Cost (kEur)	responsible lab (origine of estimates)	Quality factor	Status
Mechanics	50	IJC, UW (previous projects)	1	design
Sensors	220	KU, LLR, IFIC, IJC, TAU (offer by the vendor)	1	Prototyping
FE ASICs	330	AGH-UST, IJC, LLR (recent submissions)	2	Redesign
PCBs	52	AGH-UST, LLR, IJC, TAU (previous production)	1	
DAQ	37	IJC, TAU (FCAL experience)	1	
Power supplies	40	AGH-UST, IJC, TAU (current offers)	1	
Tooling	55	IJC, IFIC, TAU	1	
Tungsten	60	LLR, TAU (offer by the vendor)	1	
Auxiliary components	50	experience from previous projects	1	
Total sum	894			

funding to cover the costs for contact gluing including the necessary tools.
In addition, TAU together with the DESY and Freiburg University groups and other participants from Israel and Germany recently applied to the German-Israeli Project Cooperation (DIP) in the 2022 call. If successful, some funds will be dedicated to the shortfalls in the ECAL-P funding, if necessary.
ECAL-E collaborators in LUXE are also involved in the CALICE SiW calorimeter prototype effort. At the moment it can be assumed that the funding in the next two to three years will be continued at the current level in the frame of the base funding for CALICE and Linear Collider activities. The person-power situation is such that there are at the moment around ten senior researchers and engineers, one postdoc, four PhD students and one master student, and the expectation is that the same level of manpower will remain available for the next two or three years. A positive development towards a Higgs factory as well as the creation of the French-German lab DMLAB, may lead to an improvement of the situation. Currenly available is the CALICE prototype ECAL, covering a fiducial area of $18 \times 18\,\mathrm{cm}^2$, fully equipped with sensors, FE electronics and DAQ. The installation of this ECAL in LUXE would need only a small amount of additional funding. For a full coverage of ECAL-E, a second and a third stack of the same size has to be added, for which additional 430 kEuro are needed. This amount of funding is included in Table 3.

9.2 Schedule and milestones

The schedules for the construction of ECAL-E and ECAL-P are shown in Fig. 21 and Fig. 22.

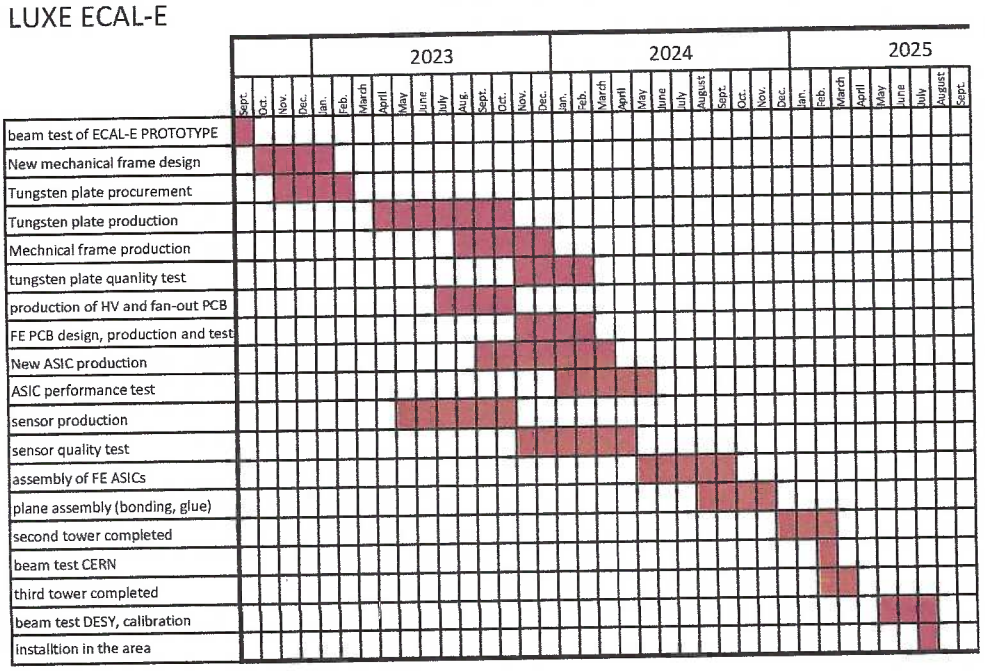

Figure 21: The time schedule for the construction, test and commissioning of the ECAL-E.

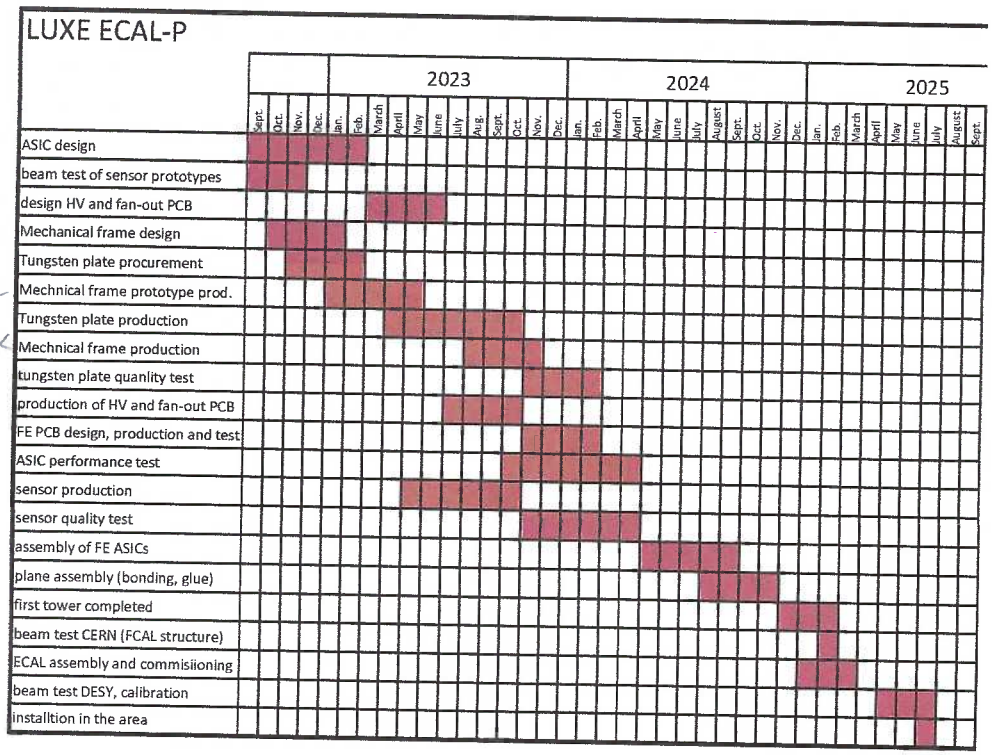

Figure 22: The time schedule for the construction, test and commissioning of the ECAL-P.

9.3 Risk management

There are two elements which may impact the time-line and the costs of ECAL-P construction. One pertains to the sensors, the other to the readout delivery.
The impact on the costs and the timeline of the ECAL-P is negligible as the sensors prices are based on current offers by Hamamatsu. The funding is not yet fully guaranteed for TAU. The other labs are still in the stage of the preparation of applications for funding. A better assessment will be known in December 2022. The expectation is that, if the LUXE project goes ahead, shortfalls in funding if any, will be covered potentially by request of extra support from TAU research funds, if not from DIP.
The production of the FEB chips is the highest risk enterprise. The main reason is funding, which is not yet guaranteed, and expected delays in chip production which presently affects the whole semiconductor-industry. Time delays of the order of 6 months may be expected. Another factor related to the chip production is an increase in pricing which may be of the order of 25% (included in price estimate). As a mitigating action, for ECAL-P the existing FLAME boards will be used for testing purposes. According to the present schedule, that would give an extra 9 months for completing the production and testing of the FLAXE readout boards. ECAL-E can, in case of major delays in ASIC production only partially assembled. In the worst case scenario, where the lack of funding would prevent the delivery of ECAL-P on time for the phase-0 data taking, the existing ECAL-E will be used on the positron side, leaving the electron side uninstrumented for the γ-laser runs. **[HA: As of March 2022, the ECAL-P team is developing a strategy to mitigate the effects of the present political crisis.]**
An attempt to summarise the risks is presented in Table 4.

Table 4: Risk description, potential impact on cost and schedule, probability to occur and strategy on how to mitigate the risk.

Description	Cost	Schedule	Prob.	Strategy
FEB chip production	±10%	25% to 35%	30%	Adapt existing FLAME readout

9.4 Responsibilities

Each institute or university will be responsible for a component of ECAL-E and ECAL-P, as shown in Table 5. A prototype of ECAL-E (CALICE Prototype) has been operated in test-beams at DESY and CERN. The Data analysis is ongoing. Tests with additional towers will need further system tests. To study the performance of sensors and ECAL-P towers, and finally a full system test and calibration, measurements will be done in the test-beam. These campaigns will be organised and funded as a joint effort.
The installation and commissioning of ECAL-E and ECAL-P will again be done in a joint effort. as described in the resource loaded schedule for ECAL-P as example, in appendix A.

Table 5: The participating institutes and their main responsibilities in the ECAL-E and ECAL-P construction.

Institute/University	contribution to ECAL-E
IFIC	contacts of sensors pads with read-out traces using conductive glue, sensors
IJC	sensors, readout, DAQ, PCB
KU	sensors, contact to Hamamatsu
LLR	sensors, PCB, assemly, tools, precise tungsten plates
Institute/University	**contribution to ECAL-P**
AGH-UST	FE-ASICs development and production, DAQ
ISS	slow control, software, computing infrastructure
TAU	sensors, assembly of detector planes, DAQ
UW	mechanical frame, precise tungsten plates

what does it mean ?!

10 Further tests planned

10.1 Test of components and the whole system in the beam

Studies of sensor response of a silicon pad sensor prototype to electrons with energy in the range of 1 to 5 GeV have been performed in the DESY II electron beam end in November 2021. A picture of the set-up is shown in Fig. 23. The detector box with the sensors under study is located downstream of the pixel telescope used to measure the beam-electron trajectory. Due to an unexpected ESD event early on in the test campaign, the trigger synchronisation between the telescope and the sensors was lost and no detailed scanning of the sensor response as a function of the electron impact could be studied. The preliminary results of the signal distribution in a silicon pad sensors is shown in Fig. 24. As can be seen a clear signal of minimum ionising particles is visible, well separated from the noise. The size of the signal matches the expectations from the energy deposited by the relativistic electrons in the sensor material. Note that zero-suppression is applied at the readout level with a threshold of 2σ, σ being the pedestal width, above the pedestal mean value. The signal distributions measured for several pads are fitted with a convolution of a Landau distribution with a Gaussian, and the most probable value, μ_{Landau}, is determined. The distributions of the μ_{Landau} values for the silicon sensor, are shown in Fig. 25. The width of the convoluted Gaussian comes out to be compatible with the pedestal width (about 1 ADC count). Within uncertainties the distribution of μ_{Landau} as a function of the pad number is uniform. What do you mean?! I would rather write it is Gaussian. This is not shown! One could even quote the width from the fit in Fig. 25 These tests will be repeated in fall 2022 to perform a detailed scanning of the sensors uniformity, cross talk and edge effects using the telescope.

The DAQ of ECAL-E and ECAL-P will be integrated into the test-beam EUDAQ system with other LUXE detectors in the test-beam.

For large values of ξ where the multiplicity of positrons may reach up 10^4 particles, there is a risk that the ECAL-P sensors or/and the front-end boards will loose their linear behaviour. The effect of these potentially high charge depositions will be studied in the recently completed DUAL HIGGINS high-power laser facility of Prof. Victor Malka at Weizmann Institute, where up to 10^7 electrons of of 0.7 GeV (with 5% energy spread) can

Figure 23: The test-beam set-up for the measurements of the sensor response. Left in the foreground is the detector box with the sensors and FE-electronics inside. In the background right the pixel telescope ~~is shown~~, used to measure the electron trajectory.

on the is

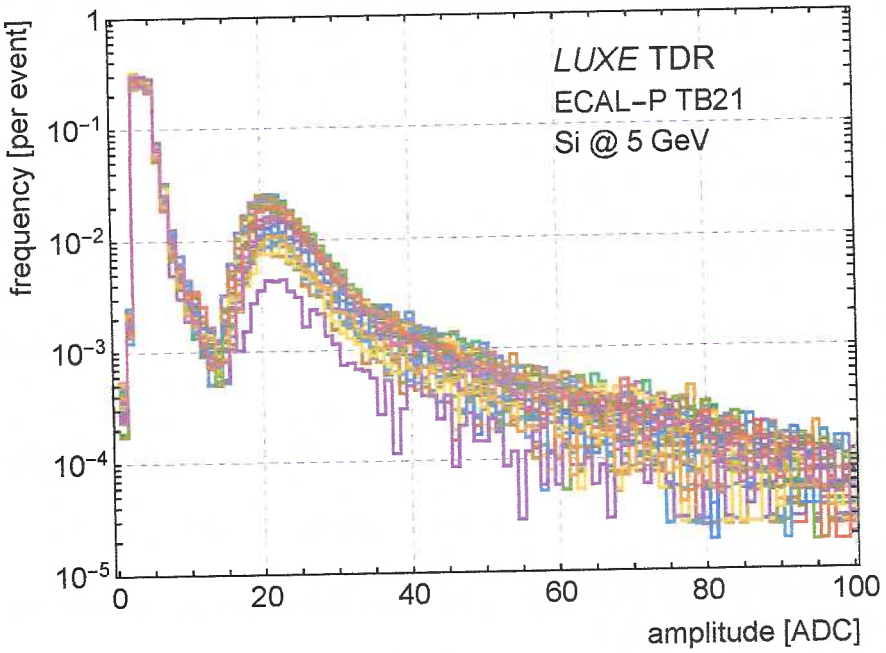

distributions

Figure 24: Response of pads in the 500 μm thick silicon sensor to electrons of 5 GeV.

different

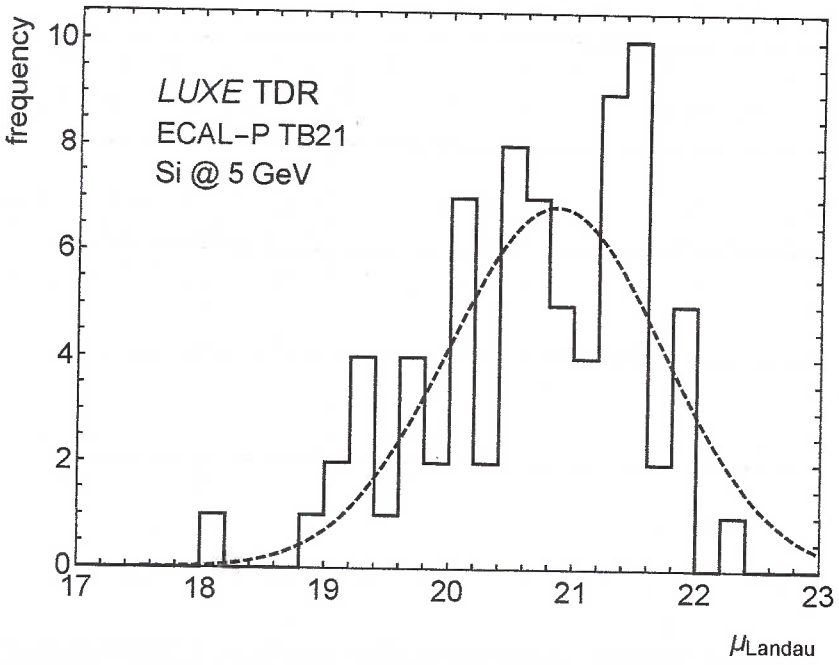

75 pads ?
Where this number comes from ?

Figure 25: Distribution of the most probable value, μ_{Landau}, from from fitting a convolution of a Landau and a Gaussian functions to spectra measured in pads in the silicon sensor.

be produced per laser shot.

Acknowledgements

This study was partly supported by the German-Israeli Foundation under grant no. I-1492-303.7/2019, the Romanian UEFISCDI agency under grant no. 16N/2019, the JINR-BMBF Programme and the Tomsk State University Development Programme («Priority-2030»).

References

[1] H. Abramowicz et al. Forward Instrumentation for ILC Detectors. *JINST*, 5:P12002, 2010.

[2] H. Abramowicz et al. Performance and Molière radius measurements using a compact prototype of LumiCal in an electron test beam. *Eur. Phys. J. C*, 79(7):579, 2019.

[3] K. Kawagoe et al. Beam test performance of the highly granular SiW-ECAL technological prototype for the ILC. *Nucl. Instrum. Meth. A*, 950:162969, 2020.

[4] T. G. Blackburn. https://github.com/tgblackburn/ptarmigan.

[5] Anthony Hartin. personal communication.

[6] S. Kulis, A. Matoga, M. Idzik, K. Swientek, T. Fiutowski, and D. Przyborowski. A general purpose multichannel readout system for radiation detectors. *JINST*, 7:T01004, 2012.

[7] S. Bugiel, R. Dasgupta, M. Firlej, T. Fiutowski, M. Idzik, M. Kopec, J. Moron, and K. Swientek. Ultra-Low Power Fast Multi-Channel 10-Bit ADC ASIC for Readout of Particle Physics Detectors. *IEEE Trans. Nucl. Sci.*, 63(5):2622–2631, 2016.

[8] P. Ahlburg et al. EUDAQ-a data acquisition software framework for common beam telescopes. *JINST*, 15(01):P01038, 2020.

[9] S. Callier, F. Dulucq, C. de La Taille, G. Martin-Chassard, and N. Seguin-Moreau. SKIROC2, front end chip designed to readout the Electromagnetic CALorimeter at the ILC. *JINST*, 6:C12040, 2011.

[10] Mykyta Shchedrolosiev. Optimization of an electromagnetic calorimeter for the luxe experiment. Taras Shevchenko National University of Kyiv, Faculty of Nuclear Physics, 2020. https://agenda.linearcollider.org/event/8107/attachments/34048/55608/main_eng.pdf.

[11] LUXE Collaboration. Technical note on Common aspects.

Appendices

A The ECAL plan for the installation

Locations:

- Experimental Area (EA)
- Control Room (CR)

List of components to be installed:

- ECAL detector, including FE PCBs
- HV and LV power supply
- Rack with crates

- FPGA cards
- DAQ Computer with ethernet connection to the rack

Expected installations prior to the one above:

- The optical table for the tracker and ECAL is available and pre-aligned
- Cables for HV and LV between detector table and rack are installed

The details of the resource loaded schedule are shown in Fig. 26.

B Changes since the CDR

Silicon sensors of $89.7 \times 89.7\,\mathrm{mm}^2$, corresponding to 16×16 pads, as produced by Hamamatsu Photonics for the CALICE Collaboration, will be used. These sensors are higher than needed, 89.7 mm instead of about 50 mm. However, since no new masks have to be produced, and the order will be done together with ECAL-E sensors, total costs will be less.

ECAL Installation						
Activity	*Duration*	*Access (*) only for extemporaneous interventions*	*ECAL people involved PH = Physicist, MEN = Mechanical Engineer, EEN = Electrical Engineer, TE = Technician*	*Man-days*		
Move the ECAL to the Area and place it on the table, move the electronics racks to the area next to the ECAL	1 day	EA	2PH, 1 TE	2		
Survey, to define the position of ECAL precisely	1/2 day	EA	1 PH, 2 survey experts from DESY/XFEL	0.5		
Connecting the cables between ECAL and the rack	1 day	EA	1 PH, 1 EEN, 1TE	1	1	
Tests of HV, LV and data connections;	3 days	EA, CR	2 PH, 1 EEN	6	3	
Test of the readout and standalone DAQ software	3 days	EA, CR	2 PH, 1 EEN	6	3	
Detector calibration	2 days	CR	2 PH	4		
Integartion in the central DAQ	2 days	CR	2 PH	4		
Sum				23.5	7	
FTE years				0.1	0.03	0.01

Figure 26: The resource loaded schedule for the installation of the ECAL. EA stands for experimental area and CR means control room.

C Quality Factor

Table 6: The list of quality factors required for quantification of the level of confidence in a price estimate.

QF1	Off-the-shelf Items for which there is a recent (< 1 year) catalog price or quote with more than one potential supplier Items that are a copy or almost identical to an existing design for which there is a recent (< 1 year) catalog price or quote with more than one potential supplier.
QF2	Items falling short of satisfying a single QF1 criterium, e.g.: - only one potential vendor; - estimate based on not completed design or design with minor modifications; - quotes > 1 year but still sufficiently reliable based on experience.
QF3	Items with quotes > 2 years Items whose cost estimates are based on a conceptual design or adapted from existing design with extensive modifications Items whose costs are estimated using physicist or engineering experience regardless of the maturity of the design.
QF4	Items that have unproven fabrication yields or for which there are unique issues e.g. a special- order item and/or a single preferred supplier.
QF5	Items that are still in a conceptual stage with no detailed specifications or design.

D All notes

This is the list of all notes and the lead editors:

- Technical infrastructure and beam instrumentation at LUXE: Louis Helary and Stewart Boogert
- Laser, interaction chambers and timing system: Matt Zepf et al.
- Laser diagnostics: Matt Zepf et al.
- Common aspects (Simulation, Data Acquisition, Data Quality and Computing): Matthew Wing, Sasha Borysov. Federico Meloni et al.
- Pixel tracker: Noam Tal Hod
- EM calorimeter: Halina Abramowicz and Wolfgang Lohmann
- Scintillation screens: Matthew Wing and John Hallford
- Cherenkov detectors: Ruth Jacobs
- Gamma Profiler: Marco Bruschi
- Gamma Spectrometer: Gianluca Sarri
- Backscattering calorimeter: Maryna Borysova
- physics performance: Beate Heinemann

.... (to be finalized)